Spin dynamics in the diluted ferromagnetic Kondo lattice model

2007 J. Phys.: Condens. Matter 19 236213

(http://iopscience.iop.org/0953-8984/19/23/236213)

IOP PUBLISHING JOURNAL OF PHYSICS: CONDENSED MATTER

J. Phys.: Condens. Matter **19** (2007) 236213 (16pp) doi:10.1088/0953-8984/19/23/236213

Spin dynamics in the diluted ferromagnetic Kondo lattice model

Avinash Singh[1,2,3], Subrat K Das[3], Anand Sharma[1] and Wolfgang Nolting[1]

[1] Institut für Physik, Humboldt-Universität zu Berlin, Newton straße. 15, D-12489 Berlin, Germany
[2] Max-Planck-Institut für Physik Komplexer Systeme, Nöthnitzer straße 38, D-01187 Dresden, Germany
[3] Department of Physics, Indian Institute of Technology, Kanpur-208016, India

E-mail: avinas@iitk.ac.in

Received 3 February 2007, in final form 13 April 2007
Published 11 May 2007
Online at stacks.iop.org/JPhysCM/19/236213

Abstract

The interplay of disorder and competing interactions is investigated in the carrier-induced ferromagnetic state of the Kondo lattice model within a numerical finite-size study in which impurity positional disorder is treated exactly. Competition between impurity spin couplings with increasing hole doping results in a strong optimization of T_c at $p \ll x$, highlighting the importance of compensation in diluted magnetic semiconductors. The estimated T_c is in good agreement with experimental results for $Ga_{1-x}Mn_xAs$ for corresponding impurity concentration, hole bandwidth, and compensation. Dilution is shown to result in a sharply enhanced density of low-energy magnon modes extended over the majority bulk spins and high-energy magnon modes localized over impurity spin clusters. The effects of these magnon properties on finite-temperature spin dynamics are studied quantitatively using a locally self-consistent magnon renormalization scheme. The large enhancement in the density of low-energy magnetic excitations results in a rapid thermal decay of magnetization, which fits well with the Bloch form $M_0(1 - BT^{3/2})$ at low temperature, with B of the same order of magnitude as obtained in recent superconducting quantum interference device (SQUID) magnetization measurements on $Ga_{1-x}Mn_xAs$ samples. Furthermore, strong cluster couplings and correlations are shown to slow down the magnetization decay and prolong magnetic ordering near T_c, as is also observed in magnetization measurements.

(Some figures in this article are in colour only in the electronic version)

1. Introduction

The discovery of ferromagnetism [1, 2] in diluted magnetic semiconductors (DMS) such as $Ga_{1-x}Mn_xAs$, with a transition temperature $T_c \simeq 110$ K for Mn concentration $x \simeq 5\%$ [2, 3], and $\simeq$ 150 K in films for x in the range 6.7%–8.5% [4, 5], has generated tremendous interest not only in view of potential technological applications but also due to the novel ferromagnetism exhibited by these systems, in which magnetic interactions between localized spins are mediated by doped carriers. The long-range oscillatory nature of the carrier-mediated spin couplings results in a variety of interesting behaviours, such as significant sensitivity of spin stiffness and transition temperature T_c on carrier concentration, competing antiferromagnetic interaction and non-collinear ordering, spin-glass behaviour, spin clustering and disorder-induced localization etc [6–20], as was recently reviewed [21, 22].

DMS such as $Ga_{1-x}Mn_xAs$ are mixed spin-fermion systems in which the $S = 5/2$ Mn^{2+} impurities replace Ga^{3+}, thereby contributing a hole to the semiconductor valence band. However, large compensation due to As antisite defects reduces the hole density p to nearly 10% Mn concentration x, which plays a key role in the stabilization of long-range ferromagnetic order, and also provides a complimentary limit to Kondo systems. The interplay between itinerant carriers in a partially filled band and the localized moments is conventionally studied within a diluted ferromagnetic Kondo lattice model (FKLM), wherein $-J\mathbf{S}_I \cdot \boldsymbol{\sigma}_I$ represents the exchange interaction between the localized magnetic impurity spin $\mathbf{S}_I$ and the itinerant electron spin $\boldsymbol{\sigma}_I$.

Recently, finite-temperature spin dynamics due to thermal spin-wave excitations has been studied in $Ga_{1-x}Mn_xAs$ samples with different Mn content (with a thickness of about 50 nm, and Mn content ranging from 2% to 6%) using SQUID (superconducting quantum interference device) magnetization measurements [23]. The temperature dependence of (low-field) spontaneous magnetization shows a nearly linear fall off, similar to earlier results [3, 4] exhibiting even a distinct concave behaviour for unannealed samples, possibly resulting from spin re-orientation transitions due to temperature-dependent magnetic anisotropies [24]. However, the spontaneous magnetization obtained using linear extrapolation from a 0.3–0.4 T magnetic field to overcome the anisotropy fields, discussed earlier for epitaxial ultra-thin Fe and FeCo films [25], is found to be described well by the Bloch form $M(T) = M_0(1 - BT^{3/2})$, with a spin-wave parameter $B \sim 1\text{–}3 \times 10^{-3}$ $K^{-3/2}$ which is about two orders of magnitude higher than for Fe and FeCo films. Post-growth annealing has been shown to significantly increase T_c, possibly due to an enhancement of carrier concentration resulting from a decrease in Mn interstitial concentration [4]. For a 50 nm sample with 6% Mn, a decrease in B from 2.7×10^{-3} $K^{-3/2}$ to 1.4×10^{-3} $K^{-3/2}$ has also been obtained upon annealing [23], with a corresponding increase in the spin-wave stiffness constant D from 53 to 71 meV $Å^2$, which is of the same order of magnitude as obtained from magnetic Kerr measurements using a pump-probe setup of standing spin waves in ferromagnetic $Ga_{1-x}Mn_xAs$ thin films [26].

In view of these recent findings of the strong thermal decay of magnetization in DMS systems, in this paper we investigate the effects of dilution on magnon excitations in the FKLM. We also study finite-temperature spin dynamics within a locally self-consistent magnon renormalization scheme equivalent to a site-dependent Tyablikov decoupling, and present the first site-dependent calculations for the temperature dependence of local impurity magnetization by explicitly incorporating the spatial feature of magnon states. As we shall see, the disorder-induced formation of low-energy extended and high-energy localized magnon modes, supported on weakly coupled majority bulk spins and strongly coupled cluster spins, respectively, results in a variety of interesting spin-dynamics behaviours, such as the rapid thermal decay of magnetization at low temperature and a tendency to prolong magnetic order near T_c due to strong cluster correlations.

Within our non-perturbative approach, finite exchange interaction, impurity concentration and disorder are treated on an equal footing. Impurity positional disorder is treated exactly by considering explicit realizations on finite-size systems and averaging over a sufficiently large number of configurations to obtain statistically reliable results.

Magnon excitations provide a composite measure of the carrier-induced spin couplings in the collinear ferromagnetic state, with negative-energy modes signalling instability due to competing antiferromagnetic (AF) interactions. Magnon properties have been studied as a function of electron density n in the conduction band and the spin-fermion coupling J within the concentrated FKLM (having a magnetic impurity at every lattice site) in the context of heavy fermion materials [27], ferromagnetic metals Gd, Tb, Dy, doped EuX [28] and manganites [29–32]. In the context of DMS, magnon properties have been studied earlier in the random phase approximation (RPA) for the impurity-band model [10] and for the diluted Hubbard model [19, 20] where disorder was treated exactly within finite-size numerical studies, and for the diluted FKLM within the virtual crystal approximation (VCA) where a uniform impurity-induced Zeeman splitting of the carrier spin bands is assumed [9], within the coherent potential approximation (CPA) [12, 33], and also for ordered impurity arrangements to make quantitative comparisons with different approximations [34]. The magnon spectrum and transition temperature have also been obtained recently for $Ga_{1-x}Mn_xAs$ and $Ga_{1-x}Mn_xN$ in terms of effective Heisenberg models with realistic exchange couplings and, within the Tyablikov decoupling formalism, both globally [35] and locally [36] self-consistent schemes have been employed for T_c calculations.

The organization of this paper is as follows. The RPA-level theory for magnon excitations in real space is derived in section 2 for a general fermion Hamiltonian, and the Goldstone-mode behaviour expected from spin–rotation symmetry is verified explicitly. Results for the diluted ferromagnetic Kondo lattice model are then discussed in section 3, with finite-temperature spin dynamics introduced in section 4. Conclusions are presented in section 5.

2. Magnon excitations

Magnons represent transverse spin fluctuations about the spontaneously broken-symmetry state and constitute gapless, low-energy excitations for magnetic systems possessing continuous spin–rotational symmetry. At low temperature, magnons therefore play an important role in diverse macroscopic properties such as the existence of long-range order, the magnitude and temperature dependences of the order parameter, the magnetic transition temperature, spin correlations etc. In the following we consider finite temperature T, and obtain magnon excitations at the RPA level where magnon interactions are neglected.

We consider the Kondo lattice model

$$H = H_0 - \frac{J}{2}\sum_I \mathbf{S}_I \cdot \boldsymbol{\sigma}_I \tag{1}$$

where H_0 represents the free-fermion part consisting generally of hopping and on-site energy terms, and the second term represents the exchange coupling between impurity spins $\mathbf{S}_I$ and fermion spins $\boldsymbol{\sigma}_I/2$ at impurity sites I. The analysis presented below is independent of details of H_0, for which several cases of interest including dilution, hopping disorder, potential disorder, and multiple bands can be considered.

Applying the approximate Holstein–Primakoff transformation from the spin-lowering (S_I^-) and spin-raising (S_I^+) operators to boson (magnon) creation and annihilation operators

$b_I^\dagger$ and b_I,

$$\begin{aligned} S_I^+ &= b_I\sqrt{2S_I} \\ S_I^- &= b_I^\dagger\sqrt{2S_I} \\ S_I^z &= S_I - b_I^\dagger b_I \end{aligned} \tag{2}$$

the Kondo lattice Hamiltonian reduces to

$$H = H_0 - \frac{J}{2}\sum_I \left[\frac{\sqrt{2S_I}}{2}\left(b_I\sigma_I^- + b_I^\dagger\sigma_I^+\right) + \left(S_I - b_I^\dagger b_I\right)\sigma_I^z\right] \tag{3}$$

where $\sigma_I^\pm \equiv \sigma_I^x \pm \mathrm{i}\sigma_I^y$ and the 'spin quantum numbers' $S_I \equiv \langle S_I^z\rangle_{\mathrm{MF}}$ refer to finite-temperature magnetizations obtained self consistently in the mean-field state. The above approximate transformation neglects quartic magnon interaction terms of order $1/S$.

Starting with a MF approximation, $\langle b_I^\dagger\rangle = \langle b_I\rangle = \langle b_I^\dagger b_I\rangle = 0$, the Hamiltonian (3) decouples into a fermion part with an impurity-field term

$$\mathcal{H}^0_{\mathrm{fermion}} = H_0 - \frac{J}{2}\sum_I S_I\sigma_I^z \tag{4}$$

and a local boson part

$$\mathcal{H}^0_{\mathrm{boson}} = \frac{J}{2}\sum_I \langle\sigma_I^z\rangle b_I^\dagger b_I \equiv \sum_I \mathcal{E}_I\, b_I^\dagger b_I, \tag{5}$$

representing the energy cost of a local spin deviation. At the MF level, the determination of the impurity and fermion magnetizations $\langle S_I^z\rangle$ and $\langle\sigma_I^z\rangle$ involves a self-consistent solution of the coupled spin-fermion problem in terms of Brillouin and Fermi functions. In the zero-temperature limit, as $S_I \equiv \langle S_I^z\rangle_{\mathrm{MF}} = S$, the impurity magnetic field seen by fermions has the same magnitude $JS/2$ on all sites, however the magnetic field $J\langle\sigma_I^z\rangle_{\mathrm{MF}}/2$ seen by impurity spins remains non-uniform due to positional disorder.

Proceeding next to transverse spin fluctuations about the MF state, we obtain the time-ordered magnon propagator for the impurity spins in terms of the corresponding boson propagator

$$\begin{aligned} \mathcal{G}_{IJ}^{+-}(t-t') &= \mathrm{i}\langle\Psi_{\mathrm{G}} \mid T[S_I^+(t)S_J^-(t')] \mid \Psi_{\mathrm{G}}\rangle \\ &= \sqrt{2S_I}\left(\mathrm{i}\langle\Psi_{\mathrm{G}} \mid T[b_I(t)b_J^\dagger(t')] \mid \Psi_{\mathrm{G}}\rangle\right)\sqrt{2S_J} \end{aligned} \tag{6}$$

at the RPA level by summing over all bubble diagrams

$\mathcal{G}_{IJ}^{+-} =$ 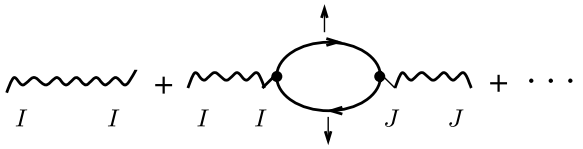

where the particle–hole bubble

$$\begin{aligned} [\chi^0(\omega)]_{IJ} &= \mathrm{i}\int\frac{\mathrm{d}\omega'}{2\pi}[G^\uparrow(\omega')]_{IJ}[G^\downarrow(\omega'-\omega)]_{JI} \\ &= \sum_{l,m}\frac{\psi_{l\uparrow}^I\psi_{l\uparrow}^J\psi_{m\downarrow}^I\psi_{m\downarrow}^J}{E_{m\downarrow}-E_{l\uparrow}+\omega}\, f_{l\uparrow}(1-f_{m\downarrow}) + \sum_{l,m}\frac{\psi_{l\uparrow}^I\psi_{l\uparrow}^J\psi_{m\downarrow}^I\psi_{m\downarrow}^J}{E_{l\uparrow}-E_{m\downarrow}-\omega}\,(1-f_{l\uparrow})f_{m\downarrow} \end{aligned} \tag{7}$$

with Fermi functions $f_{l\uparrow}$ and $f_{m\downarrow}$ involves integrating out the fermions (eigenvalues $\{E_{l\sigma}\}$ and wavefunctions $\{\psi_{l\sigma}\}$) in the broken-symmetry state. It is the particle–hole bubble $[\chi^0(\omega)]_{IJ}$ which mediates the carrier-induced impurity spin couplings in the ferromagnetic state, and the

oscillatory, long-range nature of the spin couplings is effectively controlled by the fermion band filling and the impurity field strength.

In terms of the site-diagonal zeroth-order magnon propagator

$$[\mathcal{G}^0(\omega)] = \frac{[2S_I]}{\omega - \mathcal{H}^0_{\text{boson}}} = \sum_I \frac{2S_I}{\omega - \mathcal{E}^0_I + \mathrm{i}\eta} |I\rangle\langle I| \tag{8}$$

the full magnon propagator can then be expressed as

$$\begin{aligned}[\mathcal{G}^{+-}(\omega)] &= \frac{[\mathcal{G}^0(\omega)]}{1 + \frac{J^2}{4}[\chi^0(\omega)][\mathcal{G}^0(\omega)]} \\ &= [\sqrt{2S_I}] \left(\frac{1}{\omega - [\mathcal{H}(\omega)]} \right) [\sqrt{2S_J}]\end{aligned} \tag{9}$$

in terms of a boson 'Hamiltonian'

$$[\mathcal{H}(\omega)]_{IJ} = \mathcal{E}_I \delta_{IJ} - \mathcal{E}_{IJ}(\omega) \tag{10}$$

involving the boson on-site energy

$$\mathcal{E}_I \equiv \frac{J}{2}\langle \sigma^z_I \rangle \tag{11}$$

and the boson hopping terms

$$\mathcal{E}_{IJ}(\omega) \equiv \sqrt{2S_I} \left(\frac{J^2}{4}[\chi^0(\omega)]_{IJ} \right) \sqrt{2S_J} \tag{12}$$

associated with carrier-induced spin couplings $\mathcal{J}_{IJ} = (J^2/4)[\chi^0(\omega)]_{IJ}$. While dynamical effects are, in principle, included in the magnon Hamiltonian $[\mathcal{H}(\omega)]$, we find that the ω dependence is sufficiently weak to be neglected, so that the eigenvalues and eigenvectors of $[\mathcal{H}]$ directly yield the (bare) magnon energies $\{\omega^0_l\}$ and wavefunctions $\{\phi^0_l\}$.

Equation (9) has exactly the same structure as obtained from the Tyablikov decoupling for an effective Heisenberg model with spin couplings $\mathcal{J}_{IJ} = (J^2/4)[\chi^0(\omega)]_{IJ}$, and readily yields a locally self-consistent renormalized magnon theory, as discussed in section 4. Spin-fluctuation corrections to spin couplings can be incorporated by including self-energy and vertex corrections in the particle–hole bubble within a spin–rotationally-symmetric scheme [37], but are suppressed by the factor $1/S$.

In order to obtain a zero-energy Goldstone mode consistent with spin–rotation symmetry, the energy cost of creating a local spin deviation must be exactly offset by the delocalization-induced energy gain, and the corresponding condition

$$\frac{J}{2}\langle \sigma^z_I \rangle = \mathcal{E}_I = \sum_J \frac{J^2}{4}[\chi^0(\omega = 0)]_{IJ} \cdot 2S_J \tag{13}$$

is indeed exactly satisfied. This is easily verified in the concentrated limit where translational symmetry results in plane-wave fermion states with band energies $E_{\mathbf{k}\sigma} = \epsilon_{\mathbf{k}} - \sigma J\langle S^z \rangle/2$, and the particle–hole propagator (7) simplifies to

$$\begin{aligned}\chi^0(q, \omega = 0) &= \sum_J [\chi^0(\omega = 0)]_{IJ} \\ &= \sum_{\mathbf{k}} \frac{f_{\mathbf{k}\uparrow}(1 - f_{\mathbf{k}\downarrow})}{J\langle S_z \rangle} + \frac{(1 - f_{\mathbf{k}\uparrow}) f_{\mathbf{k}\downarrow}}{-J\langle S_z \rangle} \\ &= \sum_{\mathbf{k}} \frac{(f_{\mathbf{k}\uparrow} - f_{\mathbf{k}\downarrow})}{J\langle S^z \rangle} = \frac{\langle \sigma^z \rangle}{J\langle S^z \rangle}\end{aligned} \tag{14}$$

which ensures that the required condition (13) is satisfied. Quite generally, for a spin–rotationally-invariant system, condition (13) can be derived easily from a perturbative analysis for the transverse fermion-spin density induced by small transverse impurity fields (corresponding to a small twist of the spin coordinate system), and then comparing with that expected on symmetry grounds.

The dimension of the magnon Hamiltonian $\mathcal{H}$ is $N_{\rm m}$, the number of magnetic impurities per configuration. From the $N_{\rm m}$ magnon energies $\{\omega_l^0\}$ and wavefunctions $\{\phi_l^0\}$ we evaluate the magnon density of states and the participtation ratio (PR):

$$\begin{aligned} N(\omega) &= \frac{1}{\pi}\frac{1}{N_{\rm m}}\sum_l \frac{\eta}{(\omega-\omega_l^0)^2+\eta^2} \qquad (\eta \to 0) \\ {\rm PR} &= 1 \Big/ \sum_I (\phi_l^{0I})^4, \end{aligned} \tag{15}$$

which together provide a complete picture of both spectral and spatial features of magnon states. The participation ratio provides a measure of the number of impurity spins over which the magnon state is extended. Generally, if the normalized wave function ϕ_l corresponds to a state with essentially non-zero amplitude $\phi_l^I \sim 1/\sqrt{n}$ on n sites, then PR $\sim n$. The participation ratio for magnon states can thus range between $N_{\rm m}$ for a fully extended magnon state and 1 for a site-localized magnon state. The PR thus readily allows localized magnon states (PR ~ 1) to be distinguished from extended magnon states (PR $\sim N_{\rm m}$).

We consider a simple cubic host lattice for simplicity, with periodic boundary conditions. We have considered system sizes $L = 8, 10, 12$, with the number of host lattice sites $N = L^3$ determining the dimension of the fermion Hamiltonian (4) to be diagonalized. Explicit realizations of random impurity arrangements are considered on the host lattice, for the given number $N_{\rm m}$. In all cases we consider the saturated ferromagnetic state with a filled spin-$\uparrow$ band ($N_\uparrow = N$) and doping in the spin-$\downarrow$ band which is pushed up by the impurity Zeeman field. The impurity and carrier (hole) concentrations referred to below correspond to $x = N_{\rm m}/N$ and $p = (N - N_\downarrow)/2N$, respectively.

3. Diluted Kondo lattice model

Providing a minimal description of the exchange coupling in DMS systems such as $Ga_{1-x}Mn_xAs$ between Mn impurity and carrier spins, the diluted ferromagnetic Kondo lattice model

$$H = t\sum_{i,\delta,\sigma} a_{i,\sigma}^\dagger a_{i+\delta,\sigma} + \epsilon_{\rm d}\sum_{I,\sigma} a_{I,\sigma}^\dagger a_{I,\sigma} - \frac{J}{2}\sum_I \mathbf{S}_I \cdot \boldsymbol{\sigma}_I \tag{16}$$

represents $N_{\rm m}$ magnetic impurities placed randomly on a fraction (I) of the N host sites (i). A random on-site energy ϵ_I can also be included [38] to model the local potential disorder due to non-local Coulomb potential of charged defects [22]. We consider a positive nearest-neighbour hopping t so that the host $\mathbf{k} = 0$ state lies at the top of the valence band; doped carriers (holes) go in long-wavelength states, so that small-k particle–hole processes near the Fermi energy are dominant in the carrier-induced ferromagnetic spin couplings, and therefore other details of the energy band are relatively unimportant. In the following we set $t = 1$ as the unit of energy scale. Also, as the temperature regime of interest, set by the magnon energy scale, is very low compared to the MF energy scale, in the following we have only considered the $T = 0$ case, which provides a good approximation of the low-temperature MF state.

Fermions see an effective potential disorder due to dilution—both disorder and dilution cannot be changed independently. We have therefore included an impurity on-site energy $\epsilon_{\rm d}$,

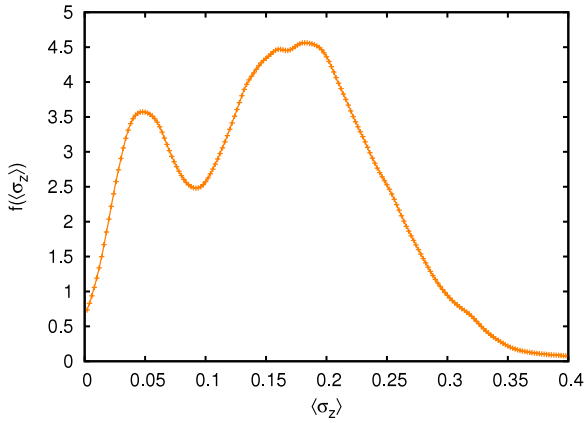

Figure 1. Distribution of fermion spin densities on impurity sites, showing significantly reduced densities in impurity-poor regions relative to their average value $\approx 2p/x$, for $J = 4$, $p \approx 2\%$, and $x \approx 20\%$.

which provides an effective control of disorder *independently* of dilution. For negative ϵ_d, the reduced impurity-site mean-field energy ($\epsilon_d + JS/2$) for spin-$\downarrow$ fermions reduces the disparity between host and impurity sites, resulting in lower effective disorder (for $\epsilon_d = -JS/2$, there is no disorder at the MF level!). The effects are quite dramatic on the magnon spectrum, showing a significant decrease in the density of low-energy modes and hence enhanced stability of the carrier-mediated ferromagnetic state. Representing the energy difference between host and impurity sites due to chemical substitution, the impurity energy ϵ_d may also be physically relevant for DMS. By tuning the shift in impurity-level position relative to the host band, the density of states can be made to resemble that obtained from band structure calculations [39].

The fermion spin polarization $\langle \sigma_I^z \rangle$ typically shows significant site variation as fermions tend to accumulate in impurity-rich regions. Figure 1 shows the distribution of fermion spin polarization on impurity sites, obtained by diagonalizing the fermion Hamiltonian (4) on a $N = 8^3$ system for 50 configurations. Besides the broad peak at the expected value of $2p/x$ corresponding to average hole density per impurity site, there is an additional peak at significantly reduced fermion spin polarization corresponding to impurity-poor regions; this introduces a new low-energy MF scale $J\langle \sigma_I^z \rangle S/2$ such that, at comparable or higher temperatures, these weakly coupled impurity spins become nearly paramagnetic. However, as we shall see, the magnon energy scale is an order of magnitude smaller than even this low-energy MF scale, indicating that the dominant spin dynamics is due to thermal excitation of the collective magnetic excitations rather than that described by the Brillouin function corresponding to single-spin excitation energies within the MF theory. A self-consistent finite-temperature mean-field analysis is therefore not required, and the $T = 0$ description provides a good approximation of the low-temperature MF state.

Figure 2(a) shows the configuration-averaged magnon density of states (DOS) for varying degree of dilution at a fixed hole doping concentration. Increasing dilution (decreasing N_m) is seen to initially broaden the magnon spectrum, but higher dilution results in significant softening of the collective excitations, with the magnon DOS peak progressively shifting to lower energy. In addition, new structure appears at higher energy, particularly at higher dilution, which is due to localized magnon states associated with strongly coupled spins in spin clusters, as was also reported in earlier studies [10, 20]. At still higher dilutions (not shown), negative-energy states appear in the magnon spectrum, indicating instability of the collinear

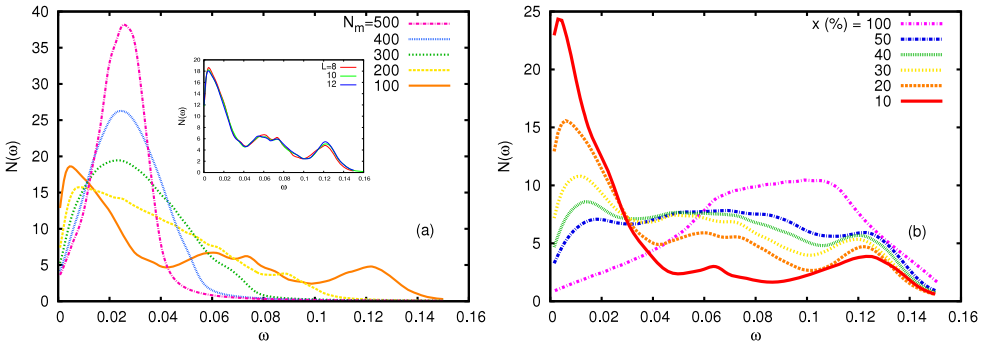

Figure 2. Strong enhancement in low-energy magnon DOS with dilution, shown for (a) fixed hole concentration $p \approx 2\%$ and (b) fixed $p/x = 1/10$. Here $J = 4$, and the system sizes considered are (a) $N = 8^3$ and (b) $N = 10^3$. Inset (a) shows (for $x \approx 20\%$) comparison of magnon DOS for different system sizes.

ferromagnetic state, in agreement with earlier magnon DOS studies carried out for a parabolic valence band [13, 22].

The asscociation of high-energy magnon states with impurity spin clusters is confirmed from figure 2(b), which shows the evolution of the magnon DOS with increasing dilution at a fixed hole concentration per impurity spin (p/x). Comparison with the concentrated case ($x = 100\%$) clearly shows that the high-energy feature continuously evolves out of the zone-boundary, spin-flip excitations at the upper end of the magnon spectrum. Figure 2(b) also highlights the sharp enhancement in density of low-energy magnetic excitations with dilution, mainly at the cost of intermediate-energy spectral weight. This strong magnon softening is due to significantly weakened bulk spin couplings, resulting from the preferential accumulation of holes in clusters and their consequent depletion from the bulk region, as indicated by a strong correlation between spin couplings and hole densities [40]. Thus, the main effect of dilution at fixed p/x is that, while the cluster spin couplings remain essentially the same as for the concentrated case, the bulk spin couplings are drastically weakened.

The correlation between spectral and spatial features of the magnon states is contained in figure 3, which shows the participation ratio (equation (15)) for different dilutions at fixed p. In addition to the magnon softening with increasing dilution, the PR plots also show the increasing localization (lower PR) of magnon states with dilution, especially for the high-energy modes which are more likely to be localized over the strongly coupled cluster spins. At high dilution ($N_{\rm m} = 100$), the low-energy magnon states are nearly extended (PR $\sim 10^2$), whereas the high-energy modes are strongly localized (PR ~ 2). Dilution-induced disorder therefore results in low-energy extended and high-energy localized magnon states, supported on weakly coupled bulk spins and strongly coupled cluster spins, respectively.

We note here that the magnon energy scale for extended modes, which essentially determines the spin dynamics in the ordered state due to thermal excitations of magnons, is very low compared to the hopping energy scale: as low as around $\sim$0.02 for the $x \approx 20\%$ case in figure 2. On the other hand, corresponding to reduced fermion polarization in impurity-poor regions, the low-energy MF scale is $J\langle\sigma_I^z\rangle S/2 \sim 0.25$. The nearly order-of-magnitude separation between these two energy scales implies, as discussed above, that the $T = 0$ calculations provide a good description of the low-temperature MF state.

Figure 4 shows the effective control of impurity disorder at fixed dilution and doping. Enhanced potential disorder with increasing J results in magnon softening (a), whereas

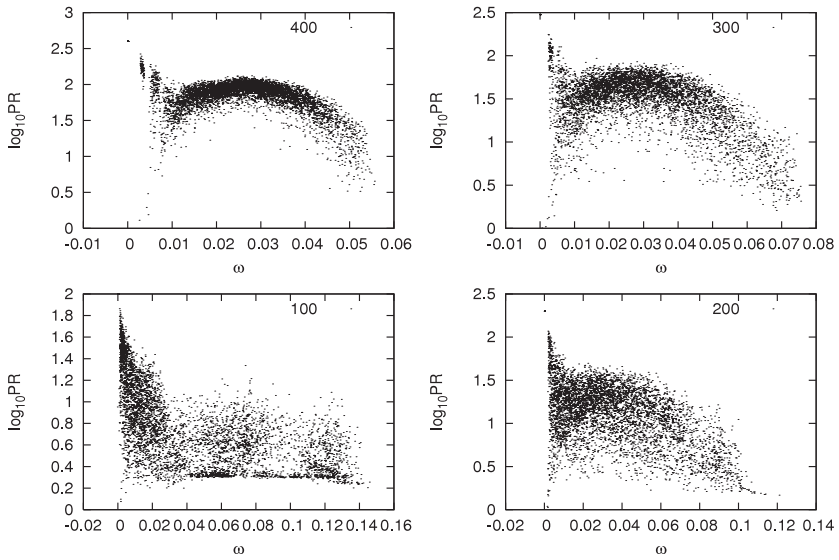

Figure 3. Participation ratio for different impurity dilutions for a $N = 8^3$ system with $J = 4$ and hole concentration $p \approx 2\%$.

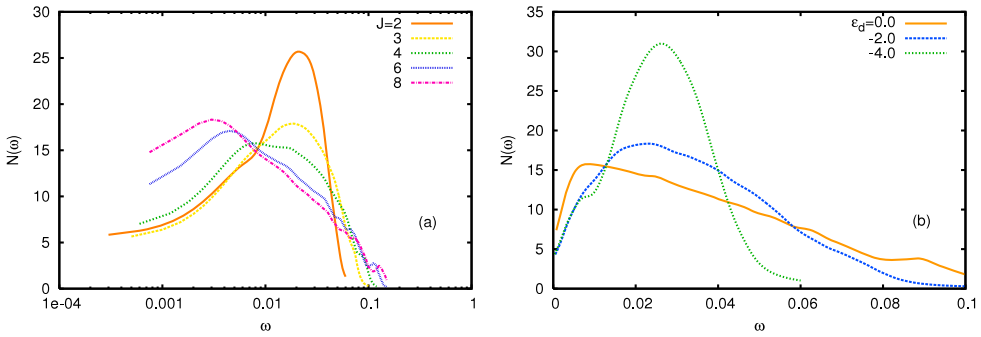

Figure 4. Magnon density of states peak shift to lower energies with increasing J and ϵ_d, showing effective control of impurity disorder independently of dilution, for a $N = 8^3$ system with $p \approx 2\%$, $x \approx 40\%$, and $\epsilon_d = 0$ (a) and $J = 4$ (b).

negative ϵ_d effectively reduces disorder in the doped spin-$\downarrow$ band and results in magnon stiffening (b), indicating stabilization of the ferromagnetic state and higher T_c. In contrast to the J^2 dependence of magnon energies within the perturbative RKKY approach, the observed magnon softening with increasing J highlights the non-perturbative character of our RPA approach.

Figure 5 shows the strong optimization of the transition temperature T_c with carrier concentration due to the characteristic competition between increasing overall magnitude of the carrier-induced spin couplings $J^2\chi^0_{IJ}$ and the increasing rapidity of its oscillation. Here we have estimated T_c from the configuration average

$$\frac{1}{T_c} = \left\langle \frac{1}{N_m} \sum_l \frac{1}{\omega_l^0} \right\rangle_c \tag{17}$$

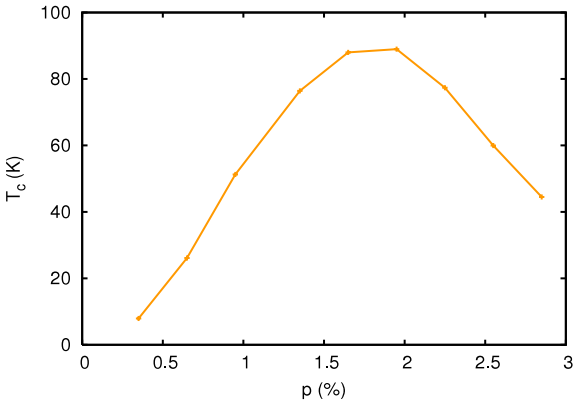

Figure 5. Optimization of T_c with hole concentration p for a $N = 10^3$ system with $J = 4$, $x = 20\%$, and carrier bandwidth $W = 12t = 10$ eV, averaged over 50 configurations.

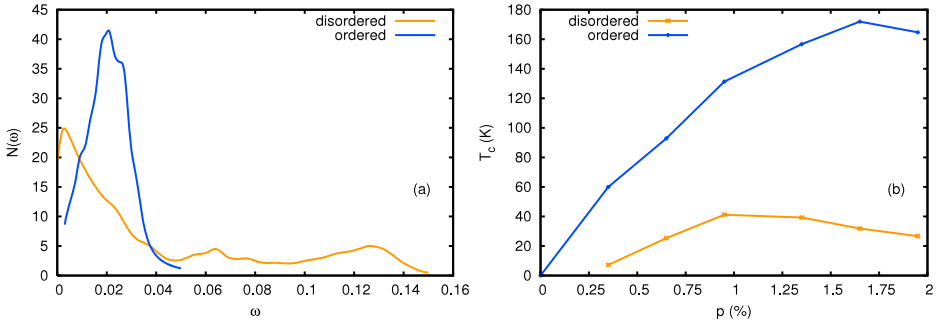

Figure 6. Comparison of magnon DOS and T_c for the ordered and disordered cases with exactly the same dilution $x = 1/8$, for a $N = 10^3$ system with $J = 4$. Here $p \approx 1.3\%$ in (a) and $W = 10$ eV in (b).

with a hole bandwidth $W = 12t = 10$ eV of the order of that of GaAs, and coupling $J = 4t = W/3 \sim 3$ eV. Experimental measurements yield $J = 1.2 \pm 0.2$ eV from core-level photoemission [41] and $J = 2.4 \pm 0.9$ eV from magneto-transport [2, 42]. Also, we have taken $x = 20\%$ for the impurity concentration (per unit cell for our sc lattice), corresponding to 5% Mn in the fcc system $Ga_{1-x}Mn_xAs$, which has 4 Ga sites per unit cell, and therefore impurity concentration $4x$ per unit cell. The peak at $p/x \sim 1/10$ shows the importance of compensation in as-grown samples of DMS systems, and the calculated T_c is in good agreement with experimental results for $Ga_{1-x}Mn_xAs$.

The effect of impurity positional disorder is highlighted in figure 6, which shows a comparison of magnon DOS and T_c for the ordered and disordered cases at the same dilution $x = 1/8$. Here the ordered case corresponds to a superlattice arrangement of impurities on alternate host lattice sites, studied earlier within a k-space sublattice-basis representation [34]. The low-energy magnon DOS is significantly enhanced in the disordered case due to weakened bulk spin couplings, resulting in substantially reduced T_c. The T_c result for the ordered case is in close agreement with earlier k-space analysis [34] in terms of spin stiffness, providing additional check on the validity of finite-size T_c calculations.

4. Finite-temperature spin dynamics

In section 3, we saw that dilution-induced disorder results in a strong enhancement in the density of low-energy magnons, with an appreciable fraction of localized modes corresponding to weakly coupled spins, as well as the formation of impurity-spin clusters supporting localized high-energy magnon modes. In order to investigate the effect of these magnon features on the finite-temperature spin dynamics quantitatively, in this section we evaluate the thermal reduction in magnetization due to magnon excitations.

We first discuss a locally self-consistent (LSC) magnon renormalization scheme for the determination of local magnetizations, which is equivalent to the site-dependent Tyablikov decoupling procedure introduced for the disordered Heisenberg ferromagnet [43], and applied recently in the $\langle S_z\rangle \to 0$ limit for T_c calculations [36]. We obtain the local magnetization from the Callen formula [44]

$$\langle S_I^z\rangle = \frac{(S-\Phi_I)(1+\Phi_I)^{2S+1} + (S+1+\Phi_I)\Phi_I^{2S+1}}{(1+\Phi_I)^{2S+1} - \Phi_I^{2S+1}} \tag{18}$$

for a quantum spin-S ferromagnet, where we have introduced site-dependent boson occupation numbers

$$\Phi_I = \frac{1}{N_m}\sum_l \frac{|\phi_l^I|^2}{e^{\beta\omega_l}-1} \tag{19}$$

which explicitly involve the boson density $(\phi_l^I)^2$. A locally self-consistent magnon renormalization scheme (in terms of the fixed FKLM spin couplings $\mathcal{J}_{IJ} = (J^2/4)[\chi^0]_{IJ}$) is then obtained if the boson Hamiltonian matrix elements (10)–(13) are self-consistently renormalized,

$$\begin{aligned}\mathcal{H}_{IJ} &= \sqrt{2\langle S_I^z\rangle}\left(\frac{J^2}{4}[\chi^0]_{IJ}\right)\sqrt{2\langle S_J^z\rangle}\\ \mathcal{H}_{II} &= \sum_{J\neq I}\left(\frac{J^2}{4}[\chi^0]_{IJ}\right)2\langle S_J^z\rangle\end{aligned} \tag{20}$$

in terms of the local magnetization $\langle S_I^z\rangle$ instead of the MF values. Together with $\mathcal{H}|\phi_l\rangle = \omega_l|\phi_l\rangle$, the coupled equations (18)–(20) then self-consistently yield the local magnetization $\langle S_I^z\rangle$ for all sites. In the translationally symmetric case this yields the usual momentum-independent magnon-energy renormalization $\omega_l = (\langle S^z\rangle/S)\omega_l^0$. In contrast to the spin Green's function representation [36, 43] for the disordered Heisenberg model involving the non-symmetric matrix $[\langle S_I^z\rangle][J_{IJ}]$, equations (18)–(20) are written in the quasi-boson representation involving the symmetric quasi-boson Hamiltonian matrix and its eigenvalues ω_l and eigenfunctions ϕ_l, and have been solved in the full temperature range $0 < T < T_c$.

In the low-temperature regime, thermal magnon renormalization is negligible ($\langle S_I^z\rangle \to S$), and the bare ($T = 0$) magnon energies ω_l^0 provide a good description of the spin dynamics. We also have $\Phi_I \ll 1$, and the magnetization equation (18) reduces to the conventional spin-wave-theory result for the site-averaged magnetization

$$\langle S_z\rangle = S - \frac{1}{N_m}\sum_I \Phi_I = S - \int d\omega \frac{N(\omega)}{e^{\beta\omega}-1}, \tag{21}$$

in terms of the bare magnon density of states $N(\omega)$. On the other hand, in an intermediate-temperature regime where $k_B T \gg \omega_l^0$ for low-energy localized modes, then $\Phi_I \sim k_B T/\omega_l^0 \gg 1$ and a nearly paramagnetic contribution $\langle S_I^z\rangle \sim \omega_l^0/k_B T$ is obtained to the local magnetization, highlighting the qualitatively different spin dynamics of the isolated, weakly coupled spins.

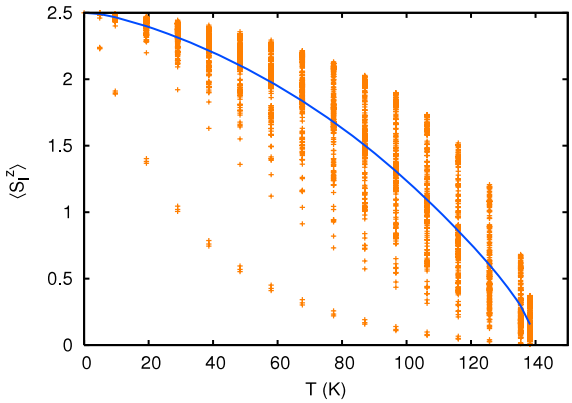

Figure 7. Temperature dependence of local magnetization $\langle S_I^z \rangle$ for all sites along with the average magnetization, obtained within the locally self-consistent magnon renormalization scheme, showing qualitatively different spin dynamics for weakly and strongly coupled spins, for a $N = 10^3$ system with $J = 4$, $x = 20\%$, $p \approx 2\%$, and $W = 10$ eV.

The result of the locally self-consistent magnon renormalization scheme (18)–(20) is shown in figure 7 for a single configuration. Starting with $\langle S_I^z \rangle = S$ for all sites, the renormalized magnon energies ω_l and wavefunctions ϕ_l are obtained by diagonalizing the renormalized magnon Hamiltonian (20), which is then updated in terms of $\langle S_I^z \rangle$ calculated from (18), (19) until self-consistency is achieved. While a large number of iterations ($\sim$50) were required near T_c, the procedure is quite fast, as the dimension of the magnon Hamiltonian (N_m) to be diagonalized in each iteration is relatively small due to dilution. The temperature dependence of local magnetization $\langle S_I^z \rangle$, plotted in figure 7 for all impurity sites, clearly shows the qualitatively different spin dynamics for weakly and strongly coupled spins *for the same magnon spectrum*, thus highlighting the role of the spatial character of magnon states. The wide range of behaviours for different spins, and therefore the different local environments, reflects the degree of complexity in a fully self-consistent magnon renormalization theory, as discussed below.

The locally self-consistent magnon renormalization scheme incorporates the spatial segregation of magnon modes. Localization of high-energy magnon modes over strongly coupled cluster spins implies that cluster spins have relatively smaller participation in the low-energy modes, resulting in smaller magnon occupation number Φ_I and higher local magnetization $\langle S_I^z \rangle$ on cluster sites at low temperature. Strong local correlations and high disordering temperature in these impurity spin clusters prolong magnetic ordering and enhance T_c, and therefore it is of interest to make a quantitative comparison with a globally self-consistent magnon renormalization scheme discussed below which deals only with the average magnon occupation number.

The globally self-consistent magnon-renormalization scheme [35] is suitable for the low-temperature regime where $\langle S_I^z \rangle \sim S$ for all sites, and also conveniently allows for configuration averaging. Here the average magnetization $\langle S_z \rangle$ is self-consistently calculated from an equation similar to (18) in terms of the configuration- and site-averaged boson occupation number

$$\Phi \equiv \langle \Phi_I \rangle = \left\langle \frac{1}{N_m} \sum_l \frac{1}{e^{\beta(\langle S_z \rangle / S)\omega_l^0} - 1} \right\rangle_c \tag{22}$$

where the bare ($T = 0$) magnon energies ω_l^0 are uniformly renormalized by the factor $\langle S_z \rangle / S$, as in the standard Tyablikov theory.

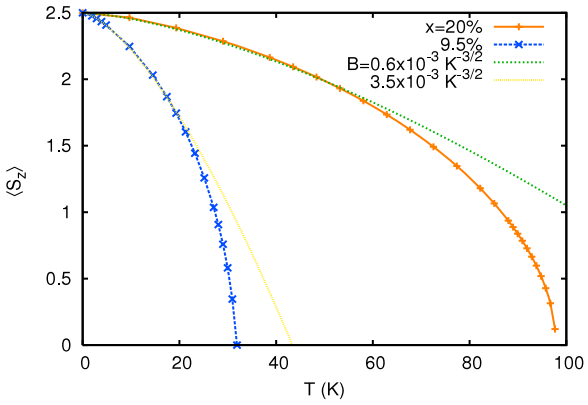

Figure 8. Configuration-averaged magnetization within the globally self-consistent magnon renormalization scheme, shown for two impurity concentrations ($x = 20\%$ and 9.5%), with $J = 4$, $W = 12t = 10$ eV, and $p/x = 1/10$, along with fits with the Bloch form $S(1 - BT^{3/2})$.

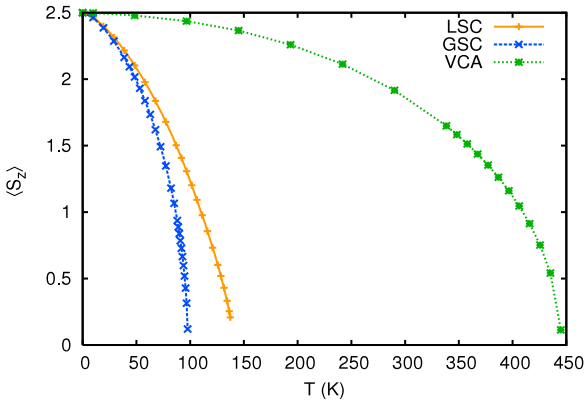

Figure 9. Comparison of the locally and globally self-consistent schemes, showing substantial enhancement in T_c due to cluster correlations when the site-dependence of local magnon occupation number and magnetization is included in the LSC scheme, for a $N = 10^3$ system (single configuration), with $J = 4$, $W = 10$ eV, $x = 20\%$, and $p \approx 2\%$. Also shown is the VCA-RPA result which drastically over-estimates T_c.

Figure 8 shows the temperature dependence of configuration-averaged magnetization obtained for $J = 4$, $p/x = 1/10$, and for two impurity concentrations—$x = 20\%$ ($N = 12^3$, 20 configurations) and $x = 9.5\%$ ($N = 10^3$, 55 configurations). Interestingly, the low-temperature behaviour of magnetization fits well with the Bloch form $S(1 - BT^{3/2})$, with $B = 0.6 \times 10^{-3}$ K$^{-3/2}$ for $x = 20\%$ and $B = 3.5 \times 10^{-3}$ K$^{-3/2}$ for $x = 9.5\%$, which is of the same order of magnitude ($\sim$1–3 $\times 10^{-3}$ K$^{-3/2}$) as obtained in SQUID magnetization measurements of $Ga_{1-x}Mn_xAs$ samples with 6% Mn concentration [23].

A comparison of the locally and globally self-consistent magnon renormalization schemes (figure 9) shows the substantial relative enhancement in T_c when the site-dependence of Φ_I and $\langle S_I^z \rangle$ is included. As discussed above, this enhancement in T_c is due to the strong local correlations and high disordering temperature in the impurity spin clusters which prolong magnetic ordering. Also shown is a comparison with Tyablikov theory (RPA) involving momentum-independent magnon-energy renormalization $\omega_{\mathbf{q}} = (\langle S_z \rangle / S)\omega_{\mathbf{q}}^0$, applied in the

virtual crystal approximation (VCA). Here the bare magnon energy is evaluated from the expression

$$\omega_q^0 = \frac{x J^2 S}{2} \left[\chi^0(0) - \chi^0(\mathbf{q})\right] \tag{23}$$

in terms of the particle–hole propagator $\chi^0(\mathbf{q})$, evaluated in the VCA ferromagnetic state with fermion band energies $E_{\mathbf{k}\sigma} = \epsilon_{\mathbf{k}} - \sigma\Delta$ and uniform Zeeman band shift $2\Delta = xJS$. Figure 9 shows that the VCA-RPA result drastically over-estimates T_c in comparison with the locally self-consistent scheme, thus highlighting the influence of disorder on the magnetization behaviour. It is the disorder-induced weakening of the majority bulk spin couplings, resulting from the preferential accumulation of holes in impurity spin clusters and their consequent depletion from bulk regions, that is responsible for the softening of low-energy magnons, rapid thermal decay of magnetization, and lower T_c.

In a further extension [45] of the VCA-RPA theory, renormalization of the Zeeman band shift $xJ\langle S_z\rangle$ has been self-consistently included in the particle–hole propagator $\chi^0(\mathbf{q})$, which determines the effective spin couplings. However, here the dynamical self-energy correction of order J^2 is neglected, which is equally important in the intermediate-coupling regime $JS \sim W$, and maintains the band splitting as $T \to T_c$ in the correlated paramagnetic state due to the presence of well-defined local moments [46].

5. Conclusions

The exact treatment of disorder in our finite-size calculations allowed for a quantitative investigation of the effects of dilution on magnon excitations in the carrier-induced ferromagnetic state of the ferromagnetic Kondo lattice model. Quantitative measures of the competition between impurity spin couplings, the stability of the ferromagnetic state, and the magnetic transition temperature could thus be obtained from our real-space analysis of magnon excitations. Furthermore, within the locally self-consistent magnon renormalization scheme, the role of both weakly coupled bulk spins and strongly coupled cluster spins, supporting extended and localized magnon excitations, respectively, could be examined on the finite-temperature spin dynamics.

Highlighting the importance of compensation in DMS systems, the strong optimization of T_c obtained with hole doping at $p/x \ll 1$ reflects the competition between increasing overall magnitude and increasing rapidity of oscillation of the carrier-induced spin couplings. The estimated T_c was found to be in good agreement with experimental results for $Ga_{1-x}Mn_xAs$ for corresponding impurity concentration, hole bandwidth, and compensation.

Comparison of the ordered and disordered cases for exactly the same dilution, with significant magnon softening and a lowering of the T_c in the disordered case, explicitly demonstrates the suppression of ferromagnetism due to dilution-induced disorder in DMS systems. The relatively milder magnon softening and robustness of the ferromagnetic state obtained for purely potential disorder [38] serves to highlight the fundamentally distinct mechanism of dilution-induced disorder. It is the preferential accumulation of holes in impurity spin clusters, and their consequent depletion from the bulk region, that is responsible for the drastic weakening (strengthening) of bulk (cluster) spin couplings, resulting in the characteristic magnon properties in a diluted magnet [40].

The large enhancement in the density of low-energy magnetic excitations was shown to be responsible for the strong thermal decay of magnetization at high dilution. While the distribution of local magnetization clearly exhibited spin-dynamics behaviour of both weakly and strongly coupled spins, the low-temperature behaviour of lattice-averaged magnetization

was found to be dominated by low-energy extended magnon states, and fitted well with the Bloch form $M_0(1-BT^{3/2})$, with B of the same order of magnitude as obtained in recent SQUID magnetization measurements on $Ga_{1-x}Mn_xAs$ samples [23]. Furthermore, the locally self-consistent magnon renormalization scheme was shown to capture the tendency of strong cluster correlations to prolong magnetic ordering near T_c. Applied to the FKLM with a small fraction of weakly coupled spins [38], the scheme highlighted both the dominant nearly paramagnetic spin dynamics of weakly coupled spins in the low-temperature regime, and the dominant spin dynamics of bulk spins near T_c. Thus a wide range of spin-dynamics behaviour involving different local environments can be studied practically using this scheme.

Finally, we mention the outstanding and interesting issue of fermion-sector renormalization, in particular of the carrier-induced spin couplings due to quantum and thermal corrections to the bare particle–hole propagator $[\chi^0(\omega)]$. In the VCA-based approaches, the effective impurity field seen by fermions is taken to vanish as $T \to T_c$, yielding RKKY-type spin couplings. However, the large separation between moment-melting and moment-disordering temperatures implies the presence of appreciable local moments even near T_c, so that fermions should continue to see impurity fields due to the slowly fluctuating, locally ordered impurity moments. Indeed, the splitting of fermion bands near T_c even for rather moderate couplings ($J/W \sim 0.2$), obtained within dynamical self-energy studies [46] of the concentrated FKLM, is precisely due to the presence of the slowly fluctuating impurity fields. It will be of interest to examine both quantum and thermal corrections to spin couplings due to self-energy and vertex corrections in $[\chi^0(\omega)]$ within a spin–rotationally invariant scheme which preserves the Goldstone mode. Studied recently for the ferromagnetic state of the Hubbard model [37], the net quantum correction can be understood essentially in terms of an exchange-energy enhancement due to fermion spectral-weight transfer. Preliminary calculation of spectral-weight transfer for the FKLM indicates a suppresion by the factor $1/S$, suggesting relatively smaller quantum corrections for large spin quantum number S.

Acknowledgments

It is a pleasure to thank M Sperl for communicating to us results prior to publication and G X Tang, J Kienert, and S Henning for helpful discussions. A Singh acknowledges support from the Alexander von Humboldt Foundation.

References

[1] Ohno H, Shen A, Matsukara F, Oiwa A, Endo A, Katsumoto S and Iye Y 1996 *Appl. Phys. Lett.* **69** 363
[2] Matsukara F, Ohno H, Shen A and Sugawara Y 1998 *Phys. Rev.* B **57** R2037
[3] Ohno H and Matsukara F 2003 *Solid State Commun.* **117** 179
[4] Ku K C, Potashnik S J, Wang R F, Chun S H, Schiffer P, Samarth N, Seong M J, Mascarenhas A, Johnston-Halperin E, Myers R C, Gossard A C and Awschalom D D 2003 *Appl. Phys. Lett.* **82** 2302
[5] Edmonds K W, Boguslawski P, Wang K Y, Campion R P, Novikov S N, Farley N R S, Gallagher B L, Foxon C T, Sawicki M, Dietl T, Nardelli M B and Bernholc J 2004 *Phys. Rev. Lett.* **92** 037201
[6] Dietl T, Haury A and d'Aubigne Y M 1997 *Phys. Rev.* B **55** R3347
Dietl T, Ohno H, Matsukara F, Cibert J and Ferrand D 2000 *Science* **287** 1019
Dietl T, Matsukara F and Ohno H 2002 *Phys. Rev.* B **66** 033203
[7] Takahashi M 1997 *Phys. Rev.* B **56** 7389
[8] Jungwirth T, Atkinson W A, Lee B H and MacDonald A H 1999 *Phys. Rev.* B **59** 9818
Lee B H, Jungwirth T and MacDonald A H 2000 *Phys. Rev.* B **61** 15606
[9] König J, Lin H-H and MacDonald A H 2000 *Phys. Rev. Lett.* **84** 5628
Schliemann J, König J and MacDonald A H 2001 *Phys. Rev.* B **64** 165201
König J, Jungwirth T and MacDonald A H 2001 *Phys. Rev.* B **64** 184423

[10] Berciu M and Bhatt R N 2001 *Phys. Rev. Lett.* **87** 107203
Berciu M and Bhatt R N 2002 *Phys. Rev.* B **66** 085207
[11] Chattopadhyay A, Das Sarma S and Millis A J 2001 *Phys. Rev. Lett.* **87** 227202
[12] Bouzerar G and Pareek T P 2002 *Phys. Rev.* B **65** 153203
[13] Schliemann J and MacDonald A H 2002 *Phys. Rev. Lett.* **88** 137201
[14] Chudnovskiy A L and Pfannkuche D 2002 *Phys. Rev.* B **65** 165216
[15] Timm C, Schäfer F and von Oppen F 2002 *Phys. Rev. Lett.* **89** 137201
Timm C and von Oppen F 2002 Physics of Semiconductors 2002 *Proc. 26th Int. Conf. on the Physics of Semiconductors (Edinburgh)* ed A R Long and J H Davies (Bristol: Institute of Physics Publishing) p H35
Timm C and von Oppen F 2003 *J. Supercond.* **16** 23
[16] Kennett M P, Berciu M and Bhatt R N 2002 *Phys. Rev.* B **65** 115308
Kennett M P, Berciu M and Bhatt R N 2002 *Phys. Rev.* B **66** 045207
[17] Alvarez G, Mayr M and Dagotto E 2002 *Phys. Rev. Lett.* **89** 277202
Alvarez G and Dagotto E 2003 *Phys. Rev.* B **68** 045202
[18] Das Sarma S, Hwang E H and Kaminski A 2003 *Phys. Rev.* B **67** 155201
Priour D J Jr, Hwang E H and Das Sarma S 2004 *Phys. Rev. Lett.* **92** 117201
[19] Singh A, Datta A, Das S K and Singh V A 2003 *Phys. Rev.* B **68** 235208
[20] Singh A 2003 *Preprint* cond-mat/0307009
[21] Bhatt R N, Berciu M, Kennet M P and Wan X 2002 *J. Supercond.* **15** 71
[22] Timm C 2003 *J. Phys.: Condens. Matter* **15** R1865
[23] Sperl M, Sadowski J, Gareev R, Wegscheider W, Weiss D and Bayreuther G 2007 Abstract from the *DPG Conference, Regensburg 2007* available at http://www.dpg-tagung.de/program/regensburg/hl23.pdf
[24] Sawicki M, Wang K-Y, Edmonds K W, Campion R P, Staddon C R, Farley N R S, Foxon C T, Papis E, Kamińska E, Piotrowska A, Dietl T and Gallagher B L 2005 *Phys. Rev.* B **71** 121302(R)
Sawicki M 2006 *J. Magn. Magn. Mater.* **300** 1
[25] Kipferl W, Sperl M, Hagler T, Meier R and Bayreuther G 2005 *J. Appl. Phys.* **97** 10B313
Sperl M, Kipferl W, Dumm M and Bayreuther G 2006 *J. Appl. Phys.* **99** 08J703
[26] Wang D M, Ren Y H, Merlin R, Dziatkowski K, Liu X, Furdyna J K and Grimsditch M 2006 *Preprint* cond-mat/0609646
[27] Sigrist M, Ueda K and Tsunetsugu H 1992 *Phys. Rev.* B **46** 175
Sigrist M, Tsunetsugu H, Ueda K and Rice T M 1992 *Phys. Rev.* B **46** 13838
[28] Donath M, Dowben P A and Nolting W 1998 *Magnetism and Electronic Correlations in Local-Moment Systems: Rare-Earth Elements and Compounds* (Singapore: World Scientfic)
[29] Furukawa N 1996 *J. Phys. Soc. Japan* **65** 1174
[30] Wang X 1998 *Phys. Rev.* B **57** 7427
[31] Yunoki S, Hu J, Malvezzi A L, Moreo A, Furukawa N and Dagotto E 1998 *Phys. Rev. Lett.* **80** 845
Dagotto E, Yunoki S, Malvezzi A L, Moreo A, Hu J, Capponi S, Poilblanc D and Furukawa N 1998 *Phys. Rev.* B **58** 6414
[32] Vogt M, Santos C and Nolting W 2001 *Phys. Status Solidi* b **223** 679
[33] Nolting W, Hickel T, Ramakanth A, Reddy G G and Lipowczan M 2004 *Phys. Rev.* B **70** 075207
[34] Das S K and Singh A 2005 *Preprint* cond-mat/0506523
[35] Hilbert S and Nolting W 2004 *Phys. Rev.* B **70** 165203
Hilbert S and Nolting W 2005 *Phys. Rev.* B **71** 113204
[36] Bouzerar G, Ziman T and Kudrnovský J 2005 *Europhys. Lett.* **69** 812
Bouzerar G, Ziman T and Kudrnovský J 2004 *Appl. Phys. Lett.* **85** 4941
Bouzerar R, Bouzerar G and Ziman T 2006 *Phys. Rev.* B **73** 024411
[37] Singh A 2006 *Phys. Rev.* B **74** 224437
[38] Singh A, Das S K, Sharma A and Nolting W 2006 *Preprint* cond-mat/0607633
[39] Bouzerar R, Bouzerar G and Ziman T 2006 *Preprint* cond-mat/0607640
[40] Singh A 2007 *Phys. Rev.* B **75** 035206
[41] Okabayashi J, Kimura A, Rader O, Mizokawa T, Fujimori A, Hayashi T and Tanaka M 1998 *Phys. Rev.* B **58** R4211
[42] Omiya T, Matsukura F, Dietl T, Ohno Y, Sakon T, Motokawa M and Ohno H 2000 *Physica* E **7** 976
[43] Hone D, Callen H B and Walker L R 1966 *Phys. Rev.* **144** 283
[44] Callen H B 1963 *Phys. Rev.* **130** 890
[45] Sun S-J and Lin H-H 2006 *Eur. Phys. J.* B **49** 403
[46] Nolting W, Rex S and Mathi Jaya S 1997 *J. Phys.: Condens. Matter* **9** 1301